Effective anisotropy of thin nanomagnets: Beyond the surface-anisotropy approach

Jean-Guy Caputo,[1,2] Yuri Gaididei,[3] Volodymyr P. Kravchuk,[4] Franz G. Mertens,[5] and Denis D. Sheka[4,*]
[1]*Laboratoire de Mathématiques, INSA de Rouen, Boîte Postale 8, 76131 Mont-Saint-Aignan Cedex, France*
[2]*Laboratoire de Physique Theorique et Modelisation, Université de Cergy-Pontoise and CNRS, Cergy-Pontoise 95011, France*
[3]*Institute for Theoretical Physics, 03143 Kiev, Ukraine*
[4]*National Taras Shevchenko University of Kiev, 03127 Kiev, Ukraine*
[5]*Physics Institute, University of Bayreuth, 95440 Bayreuth, Germany*
(Received 28 May 2007; published 15 November 2007)

We study the effective anisotropy induced in thin nanomagnets by the nonlocal demagnetization field (dipole-dipole interaction). Assuming a magnetization independent of the thickness coordinate, we reduce the energy to an inhomogeneous on-site anisotropy. Vortex solutions exist and are ground states for this model. We illustrate our approach for a disk and a square geometry. In particular, we obtain good agreement between spin-lattice simulations with this effective anisotropy and micromagnetic simulations.

DOI: 10.1103/PhysRevB.76.174428 PACS number(s): 75.10.Hk, 75.70.Ak, 75.40.Mg, 05.45.−a

I. INTRODUCTION

Magnetic nanoparticles and structures have recently attracted a growing interest for their physical properties and a number of possible applications.[1–3] For example, the vortex (ground) state of a disk-shaped nanoparticle could provide high density storage and high speed magnetic random access memory.[4] The theoretical models for these systems have been known for some time,[5,6] and include the nonlocal demagnetization field. At the microscopic level, this field is due to the dipolar interaction

$$\mathcal{H}_d = \frac{D}{2} \sum_{\substack{n,m \\ n \neq m}} \left[\frac{\boldsymbol{S_n} \cdot \boldsymbol{S_m}}{r_{nm}^3} - 3 \frac{(\boldsymbol{S_n} \cdot \boldsymbol{r_{nm}})(\boldsymbol{S_m} \cdot \boldsymbol{r_{nm}})}{r_{nm}^5} \right]. \quad (1)$$

Here, $\boldsymbol{S_n} \equiv (S_n^x, S_n^y, S_n^z)$ is a classical spin vector with fixed length S on the site $\boldsymbol{n} = (n_x, n_y, n_z)$ of a three-dimensional lattice. The summation runs over all magnets $(\boldsymbol{n}, \boldsymbol{m})$, and $\boldsymbol{r_{mn}} \equiv \boldsymbol{r_n} - \boldsymbol{r_m}$. The parameter $D = \mu_B^2 g^2$ is the strength of the long range dipolar interaction and g is the Landé factor.

In the past, analytical studies have been mainly limited to assuming a homogeneous demagnetization field distribution, uniform Stoner-Wohlfarth theory[7] and nearly uniform Brown linear analysis.[2] Recent advances in nanotechnology and computing power established the complexity of magnetization distribution in nanoparticles. For example square nanoparticles exhibit buckling states, flower states, apple states, leaf states, etc.,[8–10] when their size exceeds the single-domain limit. In disk-shaped particles, vortex states,[1,11] edge fractional vortex states, etc.,[12,13] appear. Some of these complex states can be obtained by a small perturbation of a homogeneous state. For example, Cowburn and Welland[14] showed that dipolar interactions cause flower and leaf states in square nanoparticles, which was confirmed by direct experiments.[9] However, the linear analysis does not work for topologically nontrivial states such as kinks, vortices, etc. One possibility to study these structures in nanomagnets is through the Ritz variational method. It was applied to analyze the vortex structure of the disk-shaped nanodot.[1,11] A disadvantage of this method that it limits the solution to a certain class of minimizers, so that one can usually study only one type of excitation. Linear waves are left out together with their coupling to the main excitation.

The various regimes were studied in Refs. 15–21. The important length scale is the magnetic exchange length $\ell = \sqrt{\mathsf{A}/4\pi M_S^2}$, where A is the exchange constant and M_S is the saturation magnetization. Depending on the relation between the film diameter $2R$, its thickness h, and ℓ, many scaling limits can be analyzed (see Ref. 19 for an overview). Probably the first rigorous study was made by Gioia and James,[15] who showed that for an infinitesimally thin film ($h/R \to 0$, $\ell/R \to \text{const}$), the magnetostatic energy tends to an effective two-dimensional (2D) easy-plane anisotropy energy. In this case, the ground state is a homogeneous in-plane magnetization state.[15] This effective easy-plane anisotropy has a simple magnetostatic interpretation. The sources of magnetostatic field are volume and surface magnetostatic charges. For thin structures, one can neglect the volume charges. Face surface charges contribute to the energy density as $2\pi M_z^2$, which is the same term one would get with an effective easy-plane anisotropy.[22] In the case $h/R \ll 1$ and $\ell^2 \ll 2hR\left|\ln(h/2R)\right|$, the magnetization develops edge defects, including fractional vortices.[13,20,21] This problem has a boundary constraint and an interior penalty. It is relevant for typical Permalloy ($Ni_{80}Fe_{20}$, Py) disks, where we have $h \sim 20$ nm, $2R \sim 100$ nm, and $\ell \sim 5.3$ nm.

It was shown in Refs. 18 and 19 that in the limit $h/R \to 0$ under the scaling

$$\frac{2hR}{\ell^2} \left| \ln \frac{h}{2R} \right| \to C, \quad (2)$$

the full three-dimensional (3D) micromagnetic problem reduces to a much simpler 2D variational problem, where the magnetostatic energy tends to the effective surface-anisotropy term

$$E_{\text{surf}} = \int_S (\boldsymbol{S} \cdot \boldsymbol{\tau})^2 dS, \quad (3)$$

where $\boldsymbol{\tau}$ is the local tangent vector on the surface S. In this case, the magnetization $\boldsymbol{S}$ has no out-of-plane component ($S_z = 0$) and does not develop walls and vortices.

To study nanomagnets with curling ground states, here we develop a different analytical approach. We split the dipole-dipole spin interaction (1) into two parts. The first one is an on-site anisotropy with spatially dependent anisotropy coefficients. The second part represents an effective dispersive interaction. The anisotropy interaction consists of two terms: an easy-plane anisotropy and an in-plane anisotropy. We show that the vortex state minimizes the effective in-plane anisotropy. We also show that for ultrathin nanomagnets ($h/R \to 0$), the in-plane anisotropy term reduces to the surface anisotropy (3). For the nonhomogeneous state which is our main interest, our approach is valid if

$$R \gg h \quad \text{and} \quad R \gg \ell. \tag{4}$$

In Sec. II, we introduce our discrete model together with the dipolar energy and adapt it to the plane-parallel spin-field distribution, which is our main simplification. We further simplify the model by considering only the local part of the dipolar energy, which results in an effective anisotropy. In the continuum approximation of the system, we get a local energy functional with nonhomogeneous anisotropy coefficients (see Sec. II A). The dispersive interaction is discussed in Sec. II B. To illustrate our method of effective anisotropy, we consider in Sec. III the disk-shaped nanoparticle and study its ground state spin distribution. Our simple model describes exactly the homogeneous state (see Sec. III A) and very precisely the vortex state (see Sec. III B). In Sec. IV, we confirm our analysis by numerical simulations. These are done first for the disk-shaped nanoparticle (Sec. IV A) and then for the prism-shaped one (Sec. IV B). We discuss our results in Sec. V.

II. MODEL: EFFECTIVE ANISOTROPY

We consider a ferromagnetic system described by the classical Heisenberg isotropic exchange Hamiltonian

$$\mathcal{H}_{\mathrm{ex}} = -\frac{J}{2}\sum_{\boldsymbol{n},\boldsymbol{n}'} \boldsymbol{S}_{\boldsymbol{n}}\boldsymbol{S}_{\boldsymbol{n}'}, \tag{5}$$

where the exchange integral $J>0$ and the summation runs over nearest neighbors $\boldsymbol{n}$, $\boldsymbol{n}'$. The total Hamiltonian is the sum of the exchange energy (5) and the dipolar one (1).

Our main approximation is that $\boldsymbol{S}_{\boldsymbol{n}}$ depends only on the x and y coordinates. Such a plane-parallel spin distribution is adequate for thin films with a constant thickness $h=N_z a_0$ (a_0 being the lattice constant) and nanoparticles with a small aspect ratio. The exchange interaction can be written as the sum of an intraplane $\mathcal{H}_{\mathrm{ex}}^{\mathrm{intra}}$ term and an interplane one $\mathcal{H}_{\mathrm{ex}}^{\mathrm{inter}}$,

$$\mathcal{H}_{\mathrm{ex}}^{\mathrm{intra}} = -\frac{(N_z+1)J}{2}\sum_{\boldsymbol{\nu},\boldsymbol{\nu}'} \boldsymbol{S}_{\boldsymbol{\nu}}\boldsymbol{S}_{\boldsymbol{\nu}'},$$

$$\mathcal{H}_{\mathrm{ex}}^{\mathrm{inter}} = -N_z J\sum_{\boldsymbol{\nu}} (\boldsymbol{S}_{\boldsymbol{\nu}})^2 = -N_z N_x N_y J S^2. \tag{6}$$

Here and below, the Greek index $\boldsymbol{\nu}=(n_x,n_y)$ corresponds to the XY components of the vector $\boldsymbol{n}=(n_x,n_y,n_z)$. One can see that the interplane interaction is equivalent to an on-site anisotropy. The interexchange term gives a constant contribution, so it can be omitted.

Let us consider the dipolar energy. Using the above mentioned assumption about the plane-parallel spin distribution, the dipolar Hamiltonian can be written as (see Appendix A for the details)

$$\mathcal{H}_d = -\frac{D}{2}\sum_{\boldsymbol{\nu},\boldsymbol{\mu}} [A_{\boldsymbol{\mu\nu}}(\boldsymbol{S}_{\boldsymbol{\nu}}\cdot\boldsymbol{S}_{\boldsymbol{\mu}} - 3S_{\boldsymbol{\nu}}^z S_{\boldsymbol{\mu}}^z) + B_{\boldsymbol{\mu\nu}}(S_{\boldsymbol{\nu}}^x S_{\boldsymbol{\mu}}^x - S_{\boldsymbol{\nu}}^y S_{\boldsymbol{\mu}}^y) + C_{\boldsymbol{\mu\nu}}(S_{\boldsymbol{\nu}}^x S_{\boldsymbol{\mu}}^y + S_{\boldsymbol{\nu}}^y S_{\boldsymbol{\mu}}^x)]. \tag{7}$$

Here, the sum runs only over the 2D lattice XY. All the information about the original 3D structure of our system are in the coefficients $A_{\boldsymbol{\mu\nu}}$, $B_{\boldsymbol{\mu\nu}}$, and $C_{\boldsymbol{\mu\nu}}$,

$$A_{\boldsymbol{\mu\nu}} = \frac{1}{2}\sum_{\substack{m_z,n_z \\ r_{\boldsymbol{nm}}\neq 0}} \frac{r_{\boldsymbol{mn}}^2 - 3z_{\boldsymbol{mn}}^2}{r_{\boldsymbol{mn}}^5}, \tag{8a}$$

$$B_{\boldsymbol{\mu\nu}} = \frac{3}{2}\sum_{\substack{m_z,n_z \\ r_{\boldsymbol{nm}}\neq 0}} \frac{x_{\boldsymbol{mn}}^2 - y_{\boldsymbol{mn}}^2}{r_{\boldsymbol{mn}}^5}, \tag{8b}$$

$$C_{\boldsymbol{\mu\nu}} = 3\sum_{\substack{m_z,n_z \\ r_{\boldsymbol{nm}}\neq 0}} \frac{x_{\boldsymbol{mn}}y_{\boldsymbol{mn}}}{r_{\boldsymbol{mn}}^5}. \tag{8c}$$

To gain insight into the anisotropic properties of the system, we represent the dipolar energy (7) as a sum

$$\mathcal{H}_d = \mathcal{H}_d^{\mathrm{loc}} + \Delta\mathcal{H}_d,$$

where

$$\mathcal{H}_d^{\mathrm{loc}} = -\frac{D}{2}\sum_{\boldsymbol{\nu}} \{\bar{A}_{\boldsymbol{\nu}}[(\boldsymbol{S}_{\boldsymbol{\nu}})^2 - 3(S_{\boldsymbol{\nu}}^z)^2] + \bar{B}_{\boldsymbol{\nu}}[(S_{\boldsymbol{\nu}}^x)^2 - (S_{\boldsymbol{\nu}}^y)^2] + 2\bar{C}_{\boldsymbol{\nu}}S_{\boldsymbol{\nu}}^x S_{\boldsymbol{\nu}}^y\} \tag{9}$$

is an effective on-site anisotropic energy and

$$\Delta\mathcal{H}_d = \frac{D}{4}\sum_{\boldsymbol{\nu},\boldsymbol{\mu}} \{A_{\boldsymbol{\mu\nu}}[(\boldsymbol{S}_{\boldsymbol{\nu}} - \boldsymbol{S}_{\boldsymbol{\mu}})^2 - 3(S_{\boldsymbol{\nu}}^z - S_{\boldsymbol{\mu}}^z)^2] + B_{\boldsymbol{\mu\nu}}[(S_{\boldsymbol{\nu}}^x - S_{\boldsymbol{\mu}}^x)^2 - (S_{\boldsymbol{\nu}}^y - S_{\boldsymbol{\mu}}^y)^2] + 2C_{\boldsymbol{\mu\nu}}(S_{\boldsymbol{\nu}}^x - S_{\boldsymbol{\mu}}^x)(S_{\boldsymbol{\nu}}^y - S_{\boldsymbol{\mu}}^y)\} \tag{10}$$

is the dispersive part of the dipolar interaction. Here, we introduce the coefficients of *effective anisotropy*

$$\bar{A}_{\boldsymbol{\nu}} = \sum_{\boldsymbol{\mu}} A_{\boldsymbol{\mu\nu}}, \quad \bar{B}_{\boldsymbol{\nu}} = \sum_{\boldsymbol{\mu}} B_{\boldsymbol{\mu\nu}}, \quad \bar{C}_{\boldsymbol{\nu}} = \sum_{\boldsymbol{\mu}} C_{\boldsymbol{\mu\nu}}. \tag{11}$$

The dipolar energy $\mathcal{H}_d^{\mathrm{loc}}$ contains only local interaction; it has a form of the anisotropy energy with nonhomogeneous $\bar{A}_{\boldsymbol{\nu}}$, $\bar{B}_{\boldsymbol{\nu}}$, $\bar{C}_{\boldsymbol{\nu}}$. In the next sections, we discuss both the local part $\mathcal{H}_d^{\mathrm{loc}}$ (see Sec. II A) and dispersive one $\Delta\mathcal{H}_d$ (see Sec. II B). For this end, we need to obtain the continuum limit of our model.

A. Continuum description

The continuum description of the system is based on smoothing the lattice model using the normalized magnetization

$$\boldsymbol{m}(\boldsymbol{r}) = \frac{g\mu_B}{a_0^3 M_S} \sum_{\boldsymbol{n}} \boldsymbol{S}_{\boldsymbol{n}} \delta(\boldsymbol{r} - \boldsymbol{r}_{\boldsymbol{n}}), \tag{12}$$

where M_S is the saturation magnetization. The exchange energy, the continuum version of Eq. (6), is

$$\mathcal{E}_{\mathrm{ex}} = \frac{1}{2}\mathsf{A}(h + a_0) \int dxdy (\boldsymbol{\nabla m})^2, \tag{13}$$

where $\mathsf{A} = JM_S^2 a_0^5 / D$ is the exchange constant.

Now let us consider the dipolar energy and use its approximate Hamiltonian (9). We need to transform the summation over the lattice to an integration over the volume. There is a singularity for $\boldsymbol{r}_{\boldsymbol{mn}} \to 0$. Using a regularization similar to the one in Ref. 23, we find (see Appendix B for details) that the local part of the dipolar energy is

$$\mathcal{E}_d = \pi M_S^2 h \int dxdy \{\mathcal{A}(x,y)[1 - 3\cos^2\theta(x,y)] + \sin^2\theta(x,y)\mathrm{Re}[\mathcal{B}(x,y)e^{2\imath[\phi(x,y)-\chi]}]\}, \tag{14}$$

where we used the angular parametrization for the magnetization: $m^z = \cos\theta$ and $m^x + im^y = \sin\theta e^{\imath\phi}$. Here and below, we dropped the *loc* superscript. One can see that the original nonlocal dipolar interaction results in an effective local anisotropy energy. The coefficients of effective anisotropy $\mathcal{A}$ and $\mathcal{B}$ are nonhomogeneous:

$$\mathcal{A}(x,y) = -\frac{2}{3} - \frac{a_0}{12h}\left[8\Theta_+(h) + 3 + \frac{3a_0^3}{(a_0^2 + h^2)^{3/2}}\right] + \frac{1}{2\pi}\int_0^{2\pi} d\alpha \left[\frac{\sqrt{P^2 + h^2} - P}{h} + \frac{a_0}{\sqrt{P^2 + h^2}} + \frac{a_0^2}{4Ph} + \frac{a_0^2 P^2}{4h(P^2 + h^2)^{3/2}}\right], \tag{15a}$$

$$\mathcal{B}(x,y) = \frac{1}{2\pi}\int_0^{2\pi} \mathcal{F}(P,h) e^{-2\imath\alpha} d\alpha, \tag{15b}$$

$$\mathcal{F}(P,h) = \frac{P - \sqrt{P^2 + h^2}}{h} - 2\left(1 + \frac{a_0}{h}\right)\ln\frac{\sqrt{P^2 + h^2} - h}{P} + \frac{a_0}{\sqrt{P^2 + h^2}} + \frac{3a_0^2}{4Ph} + \frac{a_0^2}{4h}\frac{3P^2 + 2h^2}{(P^2 + h^2)^{3/2}}, \tag{15c}$$

where the Heaviside function $\Theta_+(x)$ takes the unit value for any positive x and zero for $x \leqslant 0$. The term P is the distance from the point (x,y) to the border of the system; it depends on the azimuthal angle α and position (x,y) (see Fig. 1).

In the limiting case of the pure 2D system (monolayer with $h=0$), the total energy, normalized by the 2D area $\mathcal{S}$, takes the form

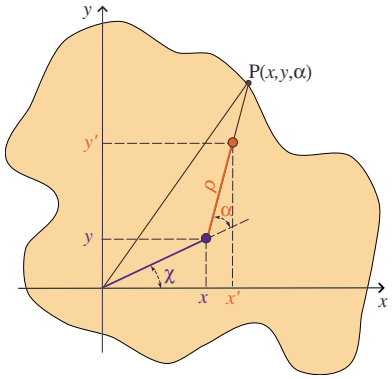

FIG. 1. (Color online) Arrangement of coordinates in the local reference frame.

$$W^{h=0} \equiv \frac{\mathcal{E}_{\mathrm{ex}} + \mathcal{E}_d}{M_S^2 \mathcal{S} a_0} = W_{\mathrm{ex}}^{h=0} + W_d^{h=0},$$

$$W_{\mathrm{ex}}^{h=0} = \frac{2\pi\ell^2}{\mathcal{S}} \int dxdy[(\boldsymbol{\nabla}\theta)^2 + \sin^2\theta(\boldsymbol{\nabla}\phi)^2],$$

$$W_d^{h=0} = \frac{\pi}{\mathcal{S}} \int dxdy\{\mathcal{A}^{h=0}(x,y)[1 - 3\cos^2\theta] + \sin^2\theta\,\mathrm{Re}[\mathcal{B}^{h=0}(x,y)e^{2\imath(\phi-\chi)}]\},$$

$$\mathcal{A}^{h=0}(x,y) = -\frac{1}{2} + \frac{a_0}{4\pi}\int_0^{2\pi}\frac{d\alpha}{P},$$

$$\mathcal{B}^{h=0}(x,y) = \frac{3a_0}{4\pi}\int_0^{2\pi}\frac{e^{-2\imath\alpha}d\alpha}{P}. \tag{16}$$

Here, the exchange length ℓ has the standard form[5]

$$\ell = \sqrt{\frac{\mathsf{A}}{4\pi M_s^2}} = a_0\sqrt{\frac{Ja_0^3}{4\pi D}}. \tag{17}$$

Note that the dipolar induced magnetic anisotropy was considered by Lévy[24] for a pure 2D spin system from a Taylor series expansion of the spin field.

The above case (16) has a rather academic interest. Below, in the paper, we consider another limit, when $h \gg a_0$. In that case, one can neglect the energy of the monolayer $W^{h=0}$. The total energy, normalized by the volume of the magnet, takes the form

$$W \equiv \frac{\mathcal{E}_{\mathrm{ex}} + \mathcal{E}_d^h}{M_S^2 \mathcal{S} h} = W_{\mathrm{ex}} + W_d, \tag{18a}$$

$$W_{\mathrm{ex}} = \frac{2\pi\ell^2}{\mathcal{S}} \int dxdy[(\boldsymbol{\nabla}\theta)^2 + \sin^2\theta(\boldsymbol{\nabla}\phi)^2], \tag{18b}$$

$$W_d = \frac{\pi}{\mathcal{S}} \int d^2x \{\mathcal{A}(x,y)[1 - 3\cos^2\theta] + \sin^2\theta \,\mathrm{Re}[\mathcal{B}(x,y)e^{2\imath(\phi-\chi)}]\}. \quad (18c)$$

The effective anisotropy constants can be expressed as follows:

$$\mathcal{A}(x,y) \approx \frac{1}{2\pi}\int_0^{2\pi} d\alpha \frac{\sqrt{P^2+h^2}-P}{h} - \frac{2}{3}, \quad (19a)$$

$$\mathcal{B}(x,y) = \frac{1}{2\pi}\int_0^{2\pi} \mathcal{F}(P,h)e^{-2i\alpha}d\alpha, \quad (19b)$$

$$\mathcal{F}(P,h) \approx \frac{P-\sqrt{P^2+h^2}}{h} - 2\ln\frac{\sqrt{P^2+h^2}-h}{P}. \quad (19c)$$

Let us discuss the magnetization distribution of the nanoparticle on a large scale. The equilibrium magnetization configuration is mainly determined by the dipolar interaction, which takes the form of an effective anisotropy (18c). The coefficient $\mathcal{A}$ determines the uniaxial anisotropy along the z axis. For a thin nanoparticle, this coefficient is always negative (with $\mathcal{A}\to -2/3$ when $h\to 0$), favoring an easy-plane magnetization distribution in agreement with the rigorous calculations.[15] The coefficient $\mathcal{B}$ is responsible for the in-plane anisotropy in the XY plane. Assume that all spins lie in the plane corresponding to the thin limit case. The preferable magnetization distribution in the XY plane is the function ϕ, minimizing the expression $\mathrm{Re}[\mathcal{B}e^{2\imath(\phi-\chi)}]$ in Eq. (18). This is

$$\phi = \chi + \frac{\pi}{2} - \frac{1}{2}\arg\mathcal{B}. \quad (20)$$

The angle (20) determines the in-plane effective anisotropy direction observed on a large scale without exchange interaction and effective uniaxial anisotropy. The analysis of the $\mathcal{B}$ term shows that the effective anisotropy favors such an in-plane spin distribution, always directed tangentially to the border near the sample edge (see Appendix C for details). This statement agrees with results for pure surface anisotropy.[12] Finer details depend on the geometry of the particle, so we need to distinguish the disk shape from the square shape.

B. Dispersive part of the dipolar interaction

In the continuum description (12), the dispersive part of the dipolar interaction (10) takes the form

$$\Delta\mathcal{E}_d = \frac{M_S^2 a_0^6}{4}\int dxdy \int dxdy' \{A(\boldsymbol{r}-\boldsymbol{r}')\{[\boldsymbol{m}(\boldsymbol{r})-\boldsymbol{m}(\boldsymbol{r}')]^2 - 3[m^z(\boldsymbol{r})-m^z(\boldsymbol{r}')]^2\} + B(\boldsymbol{r}-\boldsymbol{r}')\{[m^x(\boldsymbol{r})-m^x(\boldsymbol{r}')]^2 - [m^y(\boldsymbol{r})-m^y(\boldsymbol{r}')]^2\} + 2C(\boldsymbol{r}-\boldsymbol{r}')[m^x(\boldsymbol{r})-m^x(\boldsymbol{r}')] \times [m^y(\boldsymbol{r})-m^y(\boldsymbol{r}')]\}.$$

By applying the Fourier-transform

$$\boldsymbol{m}(\boldsymbol{r}) = \frac{1}{(2\pi)^2}\int d^2q \hat{\boldsymbol{m}}(\boldsymbol{q})e^{\imath\boldsymbol{q}\cdot\boldsymbol{r}} \quad (21)$$

and neglecting finite-size effects, the normalized dispersive part of the dipole-dipole interaction $\Delta W_d = \Delta\mathcal{E}_d/M_S^2\mathcal{S}h$ can be represented in the form

$$\Delta W_d = \frac{1}{2\pi\mathcal{S}}\int d^2q \mathfrak{G}(q)\left[-|\hat{m}_{\boldsymbol{q}}^z|^2 + \frac{|\boldsymbol{q}\cdot\hat{\boldsymbol{m}}_{\boldsymbol{q}}|^2}{q^2}\right]. \quad (22)$$

Here, $\mathbf{q}=(q_x,q_y)$ is the two-dimensional wave vector, $\hat{\boldsymbol{m}}(\boldsymbol{q})$ is the Fourier component of the two-dimensional magnetization $\boldsymbol{m}(\boldsymbol{r})$, and the function $\mathfrak{G}(q)$ is defined by the expression

$$\mathfrak{G}(q) = \frac{qh - 1 + e^{-qh}}{qh}. \quad (23)$$

Note that Eq. (22) is obtained under the assumption that the orthonormalization relation

$$\frac{1}{(2\pi)^2}\int d^2x e^{\imath(\boldsymbol{q}-\boldsymbol{q}')\cdot\boldsymbol{r}} = \delta(\boldsymbol{q}-\boldsymbol{q}')$$

takes place. Being exact for the infinite domain, this relation is only approximate for the finite-size system. For $qh\to 0$, the function (23) takes the form $\mathfrak{G}(q)\approx qh/2$. For homogeneous states, we get vanishing dispersive dipolar energy. For weakly inhomogeneous states, we expect that our effective anisotropy approach yields a good approximation, which will be verified in Sec. III for disk-shaped nanoparticles.

III. DISK-SHAPED NANOPARTICLE

Let us consider a cylindrical nanoparticle of top surface radius R and thickness h. We introduce here the aspect ratio ε and the relative distance ξ as follows:

$$\varepsilon = \frac{h}{2R}, \quad \xi = \frac{r}{R}. \quad (24)$$

Let us calculate first the effective anisotropy coefficients $\mathcal{A}$ and $\mathcal{B}$. For the circular system, the coefficients $\mathcal{A}$ and $\mathcal{B}$ depend only on ξ. We calculated analytically the coefficients $\mathcal{A}$ and $\mathcal{B}$ (see Appendix B), and these are presented in Fig. 2 and Eqs. (B8) and (B10). First, note that when $\varepsilon \gg 1$, both anisotropy constants asymptotically do not depend on ξ: $\mathcal{A}(\xi)\to 1/3$ and $\mathcal{B}(\xi)\to 0$ (see Fig. 2). The coefficient of effective uniaxial anisotropy $\mathcal{A}(\xi)$ slowly depends on ξ, namely, $\mathcal{A}(0)=[(\sqrt{1+4\varepsilon^2}-1)/2\varepsilon]-(2/3)$ and $\mathcal{A}(1)=1/3$. When the particle aspect ratio $\varepsilon \lesssim 1$, then $\mathcal{A}(\xi)<0$ [see Fig. 2(a)] and we have an effective easy-plane anisotropy. When $\varepsilon \gtrsim 1$, then $\mathcal{A}(\xi)>0$ and we have an effective easy-axis anisotropy. More details are given in Sec. III A.

In addition to the effective uniaxial anisotropy given by $\mathcal{A}(\xi)$, we have the essential $\mathcal{B}(\xi)$ term, which gives an effective in-plane anisotropy. For the disk-shaped particle, this anisotropy coefficient is always real, $\arg\mathcal{B}=0$. The value of $\mathcal{B}$ is almost 0 at the origin, but its contribution becomes important at the boundary (see Fig. 2). We obtain the following asymptotics, valid for small ε and $0.75<\xi\lesssim 1$:

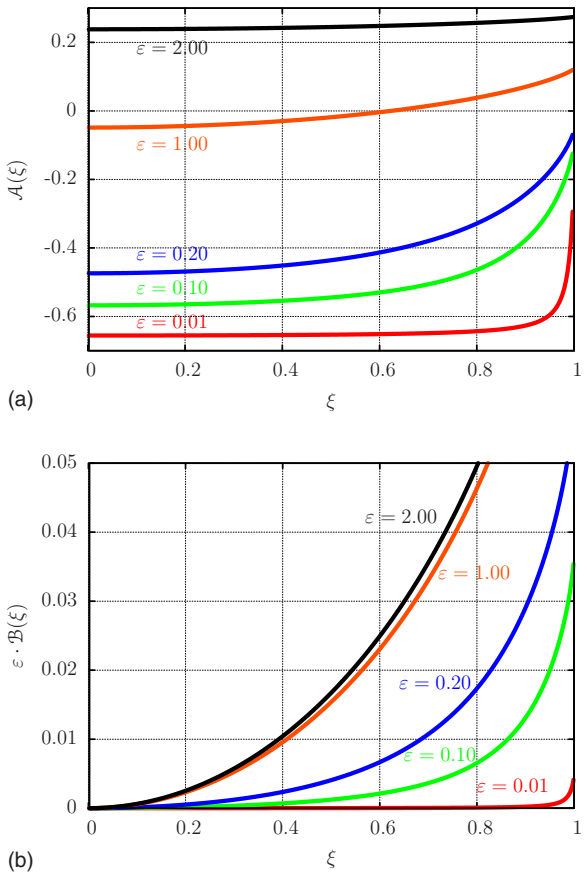

FIG. 2. (Color online) Spacial dependence of the effective anisotropy constants $\mathcal{A}$ [see Eq. (B8)] and $\mathcal{B}$ [see Eq. (B10)]. (a) The anisotropy constant $\mathcal{A}(\xi)$ vs ξ. (b) The product $\varepsilon \cdot \mathcal{B}(\xi)$ vs ξ.

$$\mathcal{B}(\xi) \approx \frac{\arctan\left(\frac{\varepsilon}{1-\xi}\right)}{\pi\xi^2} - \frac{\varepsilon(3\xi-4)}{3\pi} \ln\left(\frac{64}{\varepsilon^2+(1-\xi)^2}\right) + \frac{1-\xi}{2\pi\varepsilon} \ln\left(\frac{(1-\xi)^2}{\varepsilon^2+(1-\xi)^2}\right) \tag{25}$$

(see Appendix B). Thus, the $\mathcal{B}(\xi)$ term causes boundary effects and is responsible for the configurational anisotropy. In the limit $\varepsilon \to 0$ (more precisely, when $a_0 \ll h \ll R$), the $\mathcal{B}(\xi)$ term is concentrated near the boundary, corresponding to the surface anisotropy.

The energy of the nanodisk can be derived from Eqs. (18a)–(18c):

$$W = W_{\text{ex}} + W_d,$$

$$W_{\text{ex}} = 2\left(\frac{\ell}{R}\right)^2 \int_0^R rdr \int_0^{2\pi} d\chi[(\nabla\theta)^2 + \sin^2\theta(\nabla\phi)^2],$$

$$W_d = \int_0^{2\pi} d\chi \int_0^1 \xi d\xi[\mathcal{A}(\xi)(1-3\cos^2\theta) + \mathcal{B}(\xi)\sin^2\theta\cos 2(\phi-\chi)]. \tag{26}$$

In the next sections, we analyze the homogeneous state and the vortex state.

A. Homogeneous state

Let us consider a homogeneous magnetization along the x direction of the disk-shaped nanodot, so that $\theta=\pi/2$ and $\phi=0$. The exchange energy vanishes. The second term in the dipolar energy (26) also vanishes because of averaging on χ. The total energy W^x is then

$$W^x = 2\pi \int_0^1 \mathcal{A}(\xi)\xi d\xi = W^x_{\text{MS}}(\varepsilon) - \frac{2\pi}{3},$$

$$W^x_{\text{MS}}(\varepsilon) = \frac{4}{3\varepsilon}\{-1 + \sqrt{1+\varepsilon^2}[\varepsilon^2 K(m) + (1-\varepsilon^2)E(m)]\}, \tag{27}$$

where $m=(1+\varepsilon^2)^{-1}$ and $K(m)$ and $E(m)$ are the complete elliptic integrals of the first and the second kind, respectively.[25] The constant term $-2\pi/3$ is the isotropic contribution. The second term W^x_{MS} is the well-known magnetostatic energy of the homogeneously magnetized disk, first calculated by Joseph.[26]

If the disk is now homogeneously magnetized along the z axis, then $\theta=0$. From Eq. (26), one sees that the corresponding total energy $W^z=-2W^x$. The transition between these two homogeneous ground states occurs when $W^x=W^z$. This happens only for $W_x=0$, i.e., for $W^x_{\text{MS}}(\varepsilon_c)=2\pi/3$. This gives a critical value $\varepsilon_c \approx 0.906$, which agrees with the result by Aharoni:[27] the homogeneous easy-plane state with $\theta=\pi/2$ is realized when $\varepsilon<\varepsilon_c$, and the homogeneous easy-axis state with $\theta=0$ exists when $\varepsilon>\varepsilon_c$.

B. Vortex state

Let us consider a nonhomogeneous state of the disk-shaped particle. In this state, the system has a larger exchange energy compared to the homogeneous state. This should be compensated by the dipolar term. According to Eq. (20), the dipolar interaction always favors a spin distribution of the form

$$\phi = \chi \pm \frac{\pi}{2}, \tag{28}$$

where we take into account that the in-plane anisotropy constant $\mathcal{B}$ takes real values only. Such a configuration is called a vortex. In highly anisotropic magnets, there can exist pure planar vortices with $\theta=\pi/2$.[28] However, we consider here out-of-plane vortices, realized in "soft" materials typical of nanodisks. The out-of-plane component of the magnetization has a radial symmetric shape, and it almost does not depend on z for thin disks, $\theta=\theta(r)$. Now we can calculate the vortex energy. The vortex solution (28) is characterized by $\cos 2(\phi-\chi)=-1$, providing the minimum of the in-plane component of the dipolar energy:

$$W_d^{\text{vortex}} = W^x - 2\pi \int_0^1 \xi d\xi[3\mathcal{A}(\xi)\cos^2\theta + \mathcal{B}(\xi)\sin^2\theta]. \tag{29}$$

The exchange energy term

$$W_{\rm ex}^{\rm vortex} = 4\pi\left(\frac{\ell}{R}\right)^2 \int_0^R rdr\left[\theta'^2 + \frac{\sin^2\theta}{r^2}\right]. \tag{30}$$

Finally, the vortex energy is

$$W^{\rm vortex} = W^x + W_{\rm EP}^{\rm vortex} - F(\varepsilon),$$

$$W_{\rm EP}^{\rm vortex} = 4\pi\left(\frac{\ell}{R}\right)^2 \int_0^R rdr\left[\theta'^2 + \frac{\sin^2\theta}{r^2} + \frac{\cos^2\theta}{\ell^2}\right],$$

$$F(\varepsilon) = 2\pi\int_0^1 \xi d\xi\{[3\mathcal{A}(\xi)+2]\cos^2\theta(R\xi) + \mathcal{B}(\xi)\sin^2\theta(R\xi)\}. \tag{31}$$

Here, $W_{\rm EP}^{\rm vortex}$ coincides with the energy of the vortex in an easy-plane magnet,[29]

$$W_{\rm EP}^{\rm vortex} = 2\pi\left(\frac{\ell}{R}\right)^2 \ln\left(\frac{\pi\Lambda R^2}{\ell^2}\right), \quad \Lambda = 5.27, \tag{32}$$

and $F(\varepsilon)$ is the configurational anisotropy term. The vortex state is energetically preferable to the homogeneous state when the configurational anisotropy term exceeds the energy of the easy-plane vortex, $F(\varepsilon) > W_{\rm EP}^{\rm vortex}$. This relation allows us to calculate the critical radius R_c by solving the equation

$$2\pi\left(\frac{\ell}{R}\right)^2 \ln\left(\frac{\pi\Lambda R^2}{\ell^2}\right) = F(\varepsilon). \tag{33}$$

To calculate the integral in $F(\varepsilon)$, we use the trial function for the vortex structure

$$m^z \equiv \cos\theta = \exp(-r^2/r_v^2). \tag{34}$$

The core width depends on the disk thickness[30]

$$r_v(h) \approx \ell\sqrt{2}\sqrt[3]{1+ch/\ell}, \quad c \approx 0.39. \tag{35}$$

The relation (33) providing the border between the easy-plane and out-of-plane vortex states can be analyzed in the limit $\varepsilon \to 0$. Then $F(\varepsilon) \sim (2\pi\varepsilon/3)\ln(\pi/2\varepsilon)$, hence $R^{(c)} \approx \ell\sqrt{3/\varepsilon}$. This is in qualitative agreement with previous results.[11,31]

Let us estimate now the contribution of the dispersive part of the dipolar energy. Taking into account that for the curling state (20) the second term in Eq. (22) vanishes: $\boldsymbol{q}\cdot\hat{\boldsymbol{m}}_{\boldsymbol{q}} \equiv \widehat{\nabla\cdot\boldsymbol{m}} = 0$ and that the Fourier component of the out-of-plane component (34) has the form $\hat{m}^z = \pi r_v^2 e^{-q^2 r_v^2}$, from Eq. (22) we get

$$\Delta W_d \approx \begin{cases} \dfrac{\sqrt{\pi}}{8}\varepsilon\dfrac{r_v}{R} & \text{for } r_v \gg h \\ \dfrac{1}{2}\dfrac{r_v^2}{R^2} & \text{for } r_v \ll h. \end{cases} \tag{36}$$

Comparing Eq. (36) with Eqs. (31) and (32), and taking into account Eq. (35), one can conclude that in the limit $\varepsilon \to 0$, the dispersive part of the dipolar interaction does not change significantly the vortex stability criterion. More precisely, our effective anisotropy approximation works correctly not only for $\varepsilon \to 0$, but also for $R \gg h$ and $R \gg \ell$. Our numerical results show that it gives the vortex state as an energy minimum for disk diameters $2R \gtrsim 30\ell$.

IV. NUMERICAL SIMULATIONS

To check our effective anisotropy approximation, we performed numerical simulations. We used the publicly available three-dimensional OOMMF micromagnetic simulator code.[32] In all micromagnetic simulations, we used the following material parameters for Py: $A = 2.6\times10^{-6}$ erg/cm (using SI units $A^{\rm SI} = 2.6\times10^{-11}$ J/m), $M_s = 8.6\times10^2$ G ($M_s^{\rm SI} = 8.6\times10^5$ A/m), the damping coefficient $\eta = 0.006$, and the anisotropy has been neglected. This corresponds to an exchange length $\ell = \sqrt{A/4\pi M_s^2} \approx 5.3$ nm ($\ell^{\rm SI} = \sqrt{A/\mu_0 M_s^2}$). The mesh cells were cubic (2 nm).

We also test our effective anisotropy approach by the *original discrete spin-lattice simulator*. The spin dynamics is described by the discrete version of the Landau-Lifshitz equations with Gilbert damping

$$\frac{d\boldsymbol{S}_{\boldsymbol{n}}}{dt} = -\left[\boldsymbol{S}_{\boldsymbol{n}} \times \frac{\partial\mathcal{H}}{\partial\boldsymbol{S}_{\boldsymbol{n}}}\right] - \frac{\eta}{S}\left[\boldsymbol{S}_{\boldsymbol{n}} \times \frac{d\boldsymbol{S}_{\boldsymbol{n}}}{dt}\right], \tag{37}$$

which we consider on a 2D square lattice of size $(2R)^2$. We have assumed a plane-parallel spin distribution homogeneous along the z direction. Each lattice is bounded by a circle of radius R on which the spins are free, corresponding to a Neuman boundary condition in the continuum limit. We integrate the discrete Landau-Lifshitz equations (37) with the Hamiltonian $\mathcal{H} = \mathcal{H}_{\rm ex} + \mathcal{H}_d$ given by Eqs. (5) and (7), using a fourth-order Runge-Kutta scheme with time step $0.01/N_z$. These spin-lattice simulations were done to validate our analytical calculations for the effective anisotropy model. Throughout this work, we compared the results of the spin-lattice simulations with $\mathcal{H} = \mathcal{H}_{\rm ex} + \mathcal{H}_d$ with the results of micromagnetic simulations. We never found any noticeable difference. We present the results for a disk-shaped and a prism-shaped nanoparticle because these two geometries are the most common ones in experiments.

A. Disk-shape nanoparticle

Our effective anisotropy approximation provides the exact solution for all homogeneous states for a nanodisk. Therefore, we do not need to justify it for the homogeneous states. We consider here the vortex state. As we have analyzed before, the model can provide the preferable vortex state for disk diameters $2R > 30\ell$, which is in agreement with the model usage criterium (4). We compare the magnetization distribution in the vortex for our effective anisotropy model and for the micromagnetic simulations. Since the in-plane vortex structure is characterized by the same distribution $\phi = \chi \pm \pi/2$ for both methods, we are interested in the out-of-plane vortex profiles. We performed such a comparison for a disk of size $2R/\ell = 40$ and $h/\ell = 3$, which satisfies the criterium (4). The results are presented in Fig. 3. One can see that the vortex shape from the effective anisotropy model agrees with the one obtained from the micromagnetic simulations within 0.11 in absolute error.

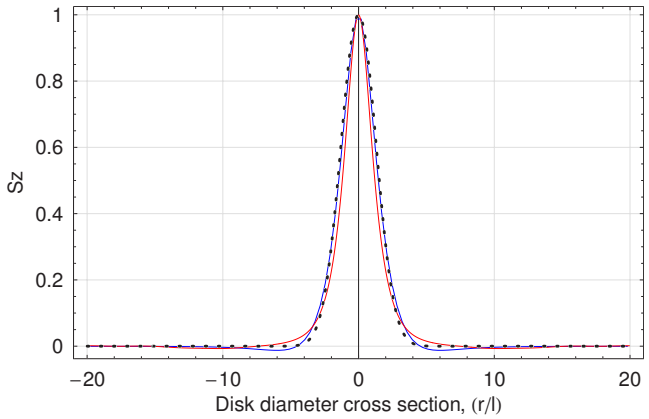

FIG. 3. (Color online) Comparison of the vortex profiles for the micromagnetic simulation and the effective anisotropy approximation for a Py nanodisk ($2R=212$ nm and $h=16$ nm). The red curve corresponds to the spin-lattice simulations for the effective anisotropy model with $\mathcal{H}=\mathcal{H}_{\rm ex}+\mathcal{H}_d^{loc}$. The blue curve corresponds to the micromagnetic simulations. The black dashed curve to the Gaussian ansatz $\cos\theta=\exp(-r^2/r_v^2)$.

B. Prism-shaped nanoparticle

Now we check the validity of the effective anisotropy approximation for the prism-shaped nanoparticle. We chose this shape because there are numerous experiments with a square geometry (for a review, see Ref. 1). We performed two types of simulations for a square-shaped nanoparticle [see Figs. 4(a) and 4(b)]. The two equilibrium magnetization distributions, obtained for the micromagnetic model and the spin-lattice simulation, agree with a very high precision.

As discussed above, the large scale distribution of the magnetization is described by Eq. (20). Calculating numerically the coefficient $\mathcal{B}$ (see Appendix C for details), we found the distribution of the configurational anisotropy lines for the square geometry. This is shown in Fig. 4(c). The comparison of Figs. 4(a)–4(c) shows that the effective anisotropy lines correspond to the magnetization direction in the main part of the system. Note that the effective anisotropy approach fails near the corners: the sharp field distribution near the prism vertices [Fig. 4(c)] is not energetically preferable when the exchange contribution is taken into account.

We can also check the validity of the effective anisotropy approach for the complicated "vortex" structure in the square geometry by comparing the distribution of the in-plane spin angle ϕ to the one given by the micromagnetic simulations. This is done in Fig. 5. The figure shows that the two different approaches agree very well. The $\phi(\chi)$ dependencies coincide within 0.11 in absolute error for $r=10\ell$ and within 0.04 for $r=20\ell$.

V. DISCUSSION

To summarize, assuming that magnetization is independent of the thickness variable z, we have reduced the magnetic energy of a thin nanodot to a local 2D inhomogeneous anisotropy. The first term $\mathcal{A}$ determines the uniaxial anisotropy along the z axis. The second term $\mathcal{B}$ gives the anisotropy in the XY plane.

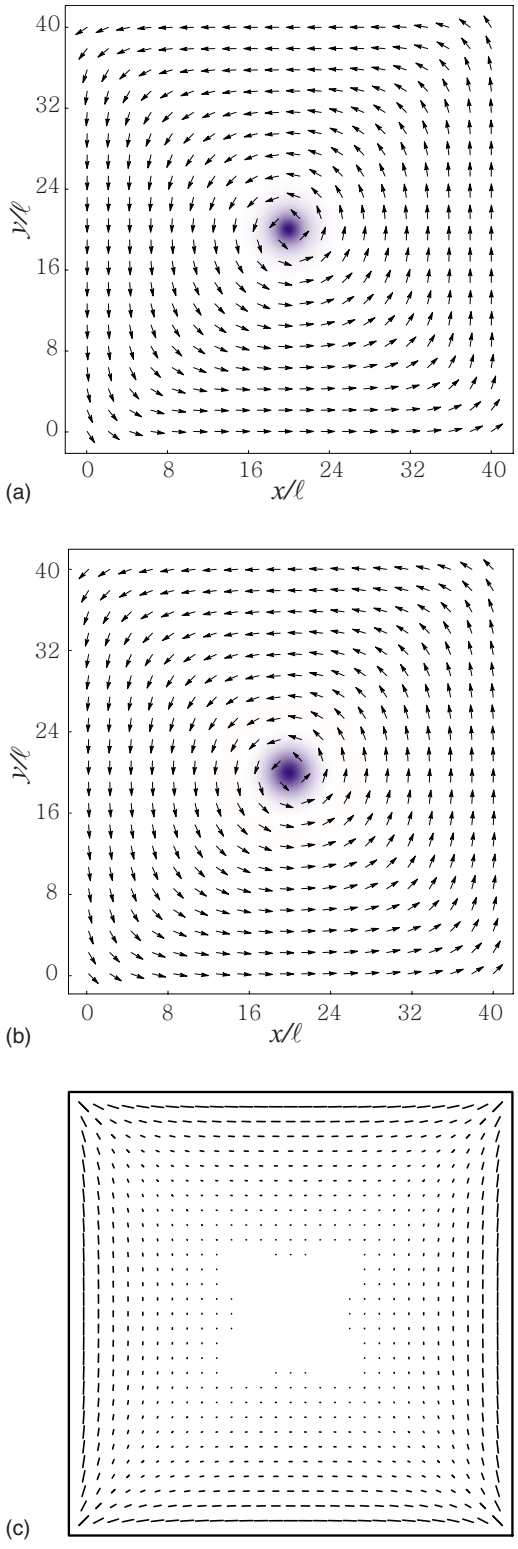

FIG. 4. (Color online) Numerical results for the vortex state Py prism (sides 212×212 nm^2 and thickness $h=16$ nm). (a) and (b) represent the spin-field distribution [(a) spin-lattice simulations for the effective anisotropy model Hamiltonian (9) and (b) micromagnetic OOMMF simulation data], and (c) the configurational anisotropy lines. These lines determine the in-plane anisotropy axis orientation, calculated from Eq. (20); the length of the lines corresponds to the anisotropy amplitude in a particular point.

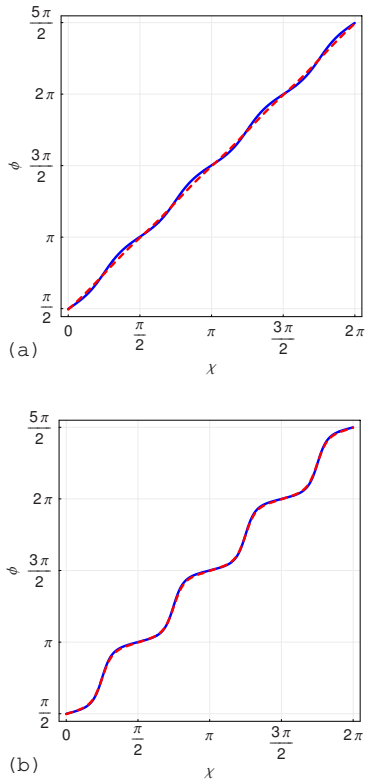

FIG. 5. (Color online) The in-plane spin angle ϕ as a function of the polar angle for the vortex state in a prism of Py of sides 212×212 nm^2 and thickness $h=16$ nm. The red dashed curves correspond to the effective anisotropy approximation; the blue solid curves to the micromagnetic simulation data. (a) Distance from the vortex center $r=10\ell$. (b) Distance from the vortex center $r=20\ell$.

For thin nanoparticles $\varepsilon \lesssim 1$, the term $\mathcal{A} \approx \text{const} < 0$ gives an effective easy-plane anisotropy. This generalizes the rigorous results obtained for infinitesimally thin films.[15] The function $\mathcal{B}(x,y)$ is localized near the edge of the particle so that spins will be tangent to the boundary. This confirms the notion of a surface edge anisotropy.[12,13]

When the nanoparticle is thick $\varepsilon \gtrsim 1$, the anisotropy constant $\mathcal{A}>0$ is again almost constant and the spins will tend to follow the z axis (easy-axis anisotropy). The in-plane anisotropy $\mathcal{B}$ depends on the thickness [see Fig. 2(a)]. The special distribution of $\mathcal{B}(x,y)$ is responsible for the volume contribution of the dipolar energy.

The above effective anisotropy approach (i) shows the nature of the effective easy-plane anisotropy and the surface anisotropy, (ii) generalizes the surface anisotropy for finite thickness, and (iii) gives a unified approach to study dipolar effects in pure 2D systems and 3D magnets of finite thickness.

It is instructive to make a link between our approach and the rigorous results obtained in Refs. 15–21. Our Eqs. (31) and (33) show that for the vortex ground state to exist, it is crucial to have both types of anisotropy: out-of-plane anisotropy and in-plane one. It is shown by Kohn and Slastikov[19] that the energy of a thin magnetic film with an accuracy up to ε^2 can be presented as the sum

$$E = E_{\text{exch}} + E_{\text{bdry}} + E_{\text{trans}} = \ell^2 \varepsilon \int_\omega |\nabla \boldsymbol{m}|^2 + \frac{\varepsilon^2 |\ln \varepsilon|}{2\pi} \int_{\partial\omega} (\boldsymbol{m}\cdot\boldsymbol{n})^2 + \varepsilon \int_\omega (m^z)^2. \tag{38}$$

Considering the limit $\varepsilon \to 0$ and $\ell^2/(\varepsilon|\ln \varepsilon|) = \text{const}$, we see from Eq. (38) that formally the last term is dominating and its contribution has to be accounted as a constraint $m^z=0$ (see Ref. 19). This constraint prevents the existence of the vortex ground state of the nanodot because the energy of the vortex in the continuum limit is infinite due to divergence at $r \to 0$. However, this divergence is removed by the out-of-plane component of the vortex, which is described by a localized function with radius of localization $r_v \sim \ell$ [see Eq. (35)]. This means that the last term E_{trans} in Eq. (38) scales like the exchange term E_{exch}. In this limit, all three terms Eq. (38) are of the same order and provide the existence of the vortex ground state.

This reduction of the nonlocal dipolar interaction to a local form is a first step toward an analytical study of nanomagnetism. We developed a method of effective anisotropy and illustrated it on a few examples. We plan to apply this method to the dynamics of vortices in nanomagnets.

ACKNOWLEDGMENTS

Yu.G., V.P.K., and D.D.S. thank the University of Bayreuth, where part of this work was performed, for kind hospitality and acknowledge the support from Deutsches Zentrum für Luft-und Raumfart e.V., Internationales Büro des BMBF in the frame of a bilateral scientific cooperation between Ukraine and Germany (Project No. UKR 05/055). J.G.C., Yu.G., and D.D.S. acknowledge support from a Ukrainian-French Dnipro grant (No. 82/240293). Yu.G. thanks the University of Cergy-Pontoise, where this work was completed. D.D.S. acknowledges the support from the Alexander von Humboldt Foundation. V.P.K. acknowledges the support from the BAYHOST project. J.G.C. thanks the Centre de Ressources Informatiques de Haute-Normandie, where part of the computations were carried out. V.P.K. and D.D.S. acknowledge the support from the Fundamental Researches State Fund of the Ukraine (Grant No. F25.2/081).

APPENDIX A: DISCRETE DIPOLAR ENERGY CALCULATIONS

Let us consider the dipolar interaction term $\mathcal{H}_d$. Using the notations

$$\frac{x_{nm}}{a_0} = n_x - m_x, \quad \frac{y_{nm}}{a_0} = n_y - m_y, \quad \frac{z_{nm}}{a_0} = n_z - m_z, \quad \rho_{\nu\mu} = \sqrt{x_{nm}^2 + y_{nm}^2}, \quad r_{nm} = \sqrt{\rho_{\nu\mu}^2 + z_{nm}^2}. \tag{A1}$$

one can rewrite this energy as follows:

$$\mathcal{H}_d = \frac{D}{2} \sum_{\substack{n,m \\ r_{nm}\neq 0}} \left\{ \frac{(\boldsymbol{S}_n \cdot \boldsymbol{S}_m)}{r_{nm}^3} - \frac{3S_n^z S_m^z z_{nm}^2}{r_{nm}^5} - \frac{6}{r_{nm}^5} S_n^z z_{nm} (S_m^x x_{nm} + S_m^y y_{nm}) - \frac{3}{r_{nm}^5} (S_n^x x_{nm} + S_n^y y_{nm})(S_m^x x_{nm} + S_m^y y_{nm}) \right\}$$

$$= D \sum_{\substack{\nu,\mu \\ \rho_{\nu\mu}\neq 0}} \{ S_\nu^z S_\mu^z K_z(\rho_{\nu\mu}) + (S_\nu^x S_\mu^x + S_\nu^y S_\mu^y) K_1(\rho_{\nu\mu}) - (S_\nu^x x_{\nu\mu} + S_\nu^y y_{\nu\mu})(S_\mu^x x_{\nu\mu} + S_\mu^y y_{\nu\mu}) K_2(\rho_{\nu\mu}) \}. \quad \text{(A2)}$$

Here, we used the obvious relations $x_{nm}=x_{\nu\mu}$ and $y_{nm}=y_{\nu\mu}$, and the basic assumption that the magnetization does not depend on the z coordinate: $\boldsymbol{S}_n=\boldsymbol{S}_\nu$ and $\boldsymbol{S}_m=\boldsymbol{S}_\mu$. This allows us to reduce the summation to the 2D lattice. The kernels K_1, K_2, and K_z contain information about the original 3D structure of our system,

$$K_1(s) = \frac{1}{2} \sum_{n_z,m_z} \frac{1}{(s^2 + z_{nm}^2)^{3/2}},$$

$$K_2(s) = \frac{3}{2} \sum_{n_z,m_z} \frac{1}{(s^2 + z_{nm}^2)^{5/2}},$$

$$K_z(s) = \frac{1}{2} \sum_{n_z,m_z} \frac{s^2 - 2z_{nm}^2}{(s^2 + z_{nm}^2)^{5/2}}. \quad \text{(A3)}$$

Taking into account that

$$S_\nu^x S_\mu^x x_{\nu\mu}^2 + S_\nu^y S_\mu^y y_{\nu\mu}^2 = \tfrac{1}{2}\rho_{\nu\mu}^2 (S_\nu^x S_\mu^x + S_\nu^y S_\mu^y) + \tfrac{1}{2}(x_{\nu\mu}^2 - y_{\nu\mu}^2)(S_\nu^x S_\mu^x - S_\nu^y S_\mu^y),$$

one can present the dipolar energy in a more symmetrical way:

$$\mathcal{H}_d = -\frac{D}{2} \sum_{\substack{\nu,\mu \\ \rho_{\nu\mu}\neq 0}} \{ K_z(\rho_{\nu\mu})(\boldsymbol{S}_\nu \cdot \boldsymbol{S}_\mu - 3S_\nu^z S_\mu^z) + K_2(\rho_{\nu\mu})(x_{\nu\mu}^2 - y_{\nu\mu}^2)(S_\nu^x S_\mu^x - S_\nu^y S_\mu^y) + 2K_2(\rho_{\nu\mu}) x_{\nu\mu} y_{\nu\mu} (S_\nu^x S_\mu^y + S_\nu^y S_\mu^x) \}. \quad \text{(A4)}$$

The total Hamiltonian is the sum of two terms (5) and (A4).

Here, we show that the main effect of the nonlocal dipolar interaction is an effective nonhomogeneous anisotropy. Using equality

$$\sum_{n,m} C_{mn} S_n S_m = \sum_n \mathcal{C}_n S_n^2 - \frac{1}{2} \sum_{n,m} C_{nm} (S_n - S_m)^2, \quad \mathcal{C}_n = \sum_m C_{nm},$$

where $C_{nm}=C_{mn}$, one can split the dipolar Hamiltonian (A4) into a local contribution and a nonlocal correction

$$\mathcal{H}_d = \mathcal{H}_d^{\mathrm{loc}} + \Delta\mathcal{H}_d \quad \text{(A5)}$$

$$\mathcal{H}_d^{\mathrm{loc}} = -\frac{D}{2} \sum_\nu \{ \bar{A}_\nu [(\boldsymbol{S}_\nu)^2 - 3(S_\nu^z)^2] + \bar{B}_\nu [(S_\nu^x)^2 - (S_\nu^y)^2] + 2\bar{C}_\nu S_\nu^x S_\nu^y \}, \quad \text{(A6)}$$

$$\Delta\mathcal{H}_d = \frac{D}{4} \sum_{\substack{\nu,\mu \\ \rho_{\nu\mu}\neq 0}} \{ K_z(\rho_{\nu\mu}) [(\boldsymbol{S}_\nu - \boldsymbol{S}_\mu)^2 - 3(S_\nu^z - S_\mu^z)^2] + K_2(\rho_{\nu\mu})(x_{\nu\mu}^2 - y_{\nu\mu}^2)[(S_\nu^x - S_\mu^x)^2 - (S_\nu^y - S_\mu^y)^2] + 4K_2(\rho_{\nu\mu}) x_{\nu\mu} y_{\nu\mu} [(S_\nu^x - S_\mu^x)(S_\nu^y - S_\mu^y)] \}. \quad \text{(A7)}$$

APPENDIX B: CONTINUUM LIMIT OF THE LOCAL DIPOLAR ENERGY

Here, we present the continuum limit of the discrete dipolar Hamiltonian (A6) corresponding to the dipolar energy

$$\mathcal{E}_d^{\mathrm{loc}} = -\frac{a_0^6 M_S^2}{2} \sum_\nu \{ \bar{A}_\nu [1 - 3(m_\nu^z)^2] + \bar{B}_\nu [(m_\nu^x)^2 - (m_\nu^y)^2] + 2\bar{C}_\nu m_\nu^x m_\nu^y \}, \quad \text{(B1)}$$

where $\boldsymbol{m}_\nu = \frac{g\mu_B}{a_0^3 M_s} \boldsymbol{S}_\nu$. Hence, the continuous magnetization vector $\boldsymbol{m}$ according to Eq. (12) takes the form $\boldsymbol{m}(\boldsymbol{r}) = \Sigma_\nu \boldsymbol{m}_\nu \delta(\boldsymbol{r} - \boldsymbol{r}_\nu)$. Here, $\bar{A}_\nu$, $\bar{B}_\nu$, and $\bar{C}_\nu$ are determined as follows:

$$\bar{A}_\nu = \sum_{\substack{\mu \\ r_{nm}\neq 0}} K_z(\rho_{\nu\mu}) = \frac{1}{2} \sum_{\substack{\mu \\ r_{nm}\neq 0}} \sum_{n_z,m_z} \frac{\rho_{\nu\mu}^2 - 2z_{nm}^2}{(\rho_{\nu\mu}^2 + z_{nm}^2)^{5/2}}, \quad \text{(B2a)}$$

$$\bar{B}_\nu = \sum_{\substack{\mu \\ r_{nm}\neq 0}} K_2(\rho_{\nu\mu})(x_{\nu\mu}^2 - y_{\nu\mu}^2) = \frac{3}{2} \sum_{\substack{\mu \\ r_{nm}\neq 0}} \sum_{n_z,m_z} \frac{x_{\nu\mu}^2 - y_{\nu\mu}^2}{(\rho_{\nu\mu}^2 + z_{nm}^2)^{5/2}}, \quad \text{(B2b)}$$

$$\bar{C}_\nu = \sum_{\substack{\mu \\ r_{nm}\neq 0}} K_2(\rho_{\nu\mu}) 2x_{\nu\mu} y_{\nu\mu} = \frac{3}{2} \sum_{\substack{\mu \\ r_{nm}\neq 0}} \sum_{n_z,m_z} \frac{2x_{\nu\mu} y_{\nu\mu}}{(\rho_{\nu\mu}^2 + z_{nm}^2)^{5/2}}. \quad \text{(B2c)}$$

The continuum version of the effective anisotropy constants (B2) can be found using a relation

$$\sum_{n_z=0}^{N_z} \sum_{m_z=0}^{N_z} F(|z_{nm}|) \approx \frac{1}{a_0^2} \int_0^h dz \int_0^h dz' F(|z - z'|) + \frac{1}{a_0} \int_0^h dz [F(|z|) + F(|h - z|)] + \frac{1}{2}[F(0) + F(|h|)] = \frac{2}{a_0^2} \int_0^h dz F(|z|)[h - z + a_0] + \frac{1}{2}[F(0) + F(|h|)], \quad h = N_z a_0 \geq 0. \quad \text{(B3)}$$

Let us start with the calculation of the coefficient $\bar{A}_\nu$ from Eq. (B2a):

$$\mathcal{A}(x,y) \equiv -\frac{a_0^4}{2\pi h}\bar{A}_{\boldsymbol{\nu}} = \frac{1}{h}(\mathcal{A}_1 + \mathcal{A}_2 + \mathcal{A}_3),$$

$$\mathcal{A}_1 = \frac{\Theta_+(h)}{2\pi} \lim_{r^\star \to 0} \int_{|\boldsymbol{r}-\boldsymbol{r}'|>r^\star} dx'dy' \times \int_0^h dz \frac{(2z^2-\rho^2)(h-z+a_0)}{(\rho^2+z^2)^{5/2}},$$

$$\mathcal{A}_2 = -\frac{a_0^4}{8\pi} \sum_{\substack{\boldsymbol{\mu} \\ r_{\boldsymbol{nm}} \neq 0}} \frac{1}{\rho_{\boldsymbol{\nu\mu}}^3} \approx \frac{a_0^2}{8\pi}\int_0^{2\pi} \frac{d\alpha}{P} - \frac{a_0}{4},$$

$$\mathcal{A}_3 = \frac{a_0^2}{8\pi}\int dx'dy' \frac{2h^2-\rho^2}{(\rho^2+h^2)^{5/2}} \approx \frac{a_0^2}{8\pi}\int_0^{2\pi} \frac{P^2 d\alpha}{(P^2+h^2)^{3/2}} - \frac{a_0^4}{4(a_0^2+h^2)^{3/2}}. \quad \text{(B4)}$$

Here, $\rho=\sqrt{(x-x')^2+(y-y')^2}$ and we used a local reference frame

$$x' = x + \rho\cos(\chi+\alpha), \quad y' = y + \rho\sin(\chi+\alpha), \quad \text{(B5)}$$

which is centered at (x,y). The Heaviside function $\Theta_+(x)$ takes the unit value for any positive x, and zero for $x \leqslant 0$; it is added here to fulfill the condition $\mathcal{A}_1 \equiv 0$ in the 2D case when $h=0$. There is a singularity in $\mathcal{A}_1$ due to the nonintegrability of the kernel K_z at $r_{\boldsymbol{nm}}=0$. To regularize it, we use a method similar to the one in Ref. 23. Specifically, we present $\mathcal{A}_1$ in the form $\mathcal{A}_1=\tilde{\mathcal{A}}_1-\mathcal{A}_0$. The coefficient $\tilde{\mathcal{A}}_1$ is a regular one:

$$\tilde{\mathcal{A}}_1 = \frac{\Theta_+(h)}{2\pi}\int dx'dy' \int_0^h dz \frac{(2z^2-\rho^2)(h-z+a_0)}{(\rho^2+z^2)^{5/2}} = -h - a_0\Theta_+(h) + \frac{1}{2\pi}\int_0^{2\pi} d\alpha \left[\sqrt{P^2+h^2} - P + \frac{a_0 h}{\sqrt{P^2+h^2}}\right].$$

The singularity is inside the $\mathcal{A}_0$ term:

$$\mathcal{A}_0 = \frac{\Theta_+(h)}{2\pi} \lim_{r^\star \to 0} \int_{\substack{|\boldsymbol{r}-\boldsymbol{r}'|<r^\star \\ z=0,z'>0}} d^2x'dz' \frac{(2z'^2-\rho^2)(h-z'+a_0)}{(\rho^2+z'^2)^{5/2}} = \frac{\Theta_+(h)}{2\pi}[(h+a_0)I_1 - I_2],$$

$$I_1 = \lim_{r^\star \to 0} \int_{\substack{|\boldsymbol{r}-\boldsymbol{r}'|<r^\star \\ z=0,z'>0}} d^2x'dz' \frac{2z'^2-\rho^2}{(\rho^2+z'^2)^{5/2}} = \lim_{r^\star \to 0} \int_{\substack{|\boldsymbol{r}-\boldsymbol{r}'|<r^\star \\ z=0,z'>0}} d^2x'dz' \frac{\partial^2}{\partial z'^2}\frac{1}{|\boldsymbol{r}-\boldsymbol{r}'|}$$

$$= \frac{1}{3}\lim_{r^\star \to 0} \int_{\substack{|\boldsymbol{r}-\boldsymbol{r}'|<r^\star \\ z=0,z'>0}} d^3x' \Delta \frac{1}{|\boldsymbol{r}-\boldsymbol{r}'|} = -\frac{4\pi}{3}\lim_{r^\star \to 0} \int_{\substack{|\boldsymbol{r}-\boldsymbol{r}'|<r^\star \\ z=0,z'>0}} d^3x' \delta(\boldsymbol{r}-\boldsymbol{r}') = -\frac{2\pi}{3},$$

$$I_2 = \lim_{r^\star \to 0} \int_{\substack{|\boldsymbol{r}-\boldsymbol{r}'|<r^\star \\ z=0,z'>0}} d^2x'dz' \frac{z'(2z'^2-\rho^2)}{(\rho^2+z'^2)^{5/2}} = \frac{4\pi}{3}\lim_{r^\star \to 0} \int_{\substack{|\boldsymbol{r}-\boldsymbol{r}'|<r^\star \\ z=0,z'>0}} d^3x' z' \delta(\boldsymbol{r}-\boldsymbol{r}') = 0. \quad \text{(B6)}$$

Finally, $\mathcal{A}_0=-[h+a_0\Theta_+(h)]/3$ and the coefficient of effective anisotropy $\mathcal{A}(x,y)$ takes the form (15a).

The coefficients $\bar{B}_{\boldsymbol{\nu}}$ and $\bar{C}_{\boldsymbol{\nu}}$ can be calculated in the same way, starting from Eq. (B2b):

$$\mathcal{B}(x,y) \equiv -\frac{a_0^4 e^{2\imath\chi}}{2\pi h}[\bar{B}_{\boldsymbol{\nu}} - \imath\bar{C}_{\boldsymbol{\nu}}] = -\frac{3a_0^4}{4\pi h}\sum_{\substack{\boldsymbol{\mu} \\ r_{\boldsymbol{nm}} \neq 0}} \rho_{\boldsymbol{\nu\mu}}^2 e^{-2\imath\alpha_{\boldsymbol{\nu\mu}}} \sum_{n_z,m_z} \frac{1}{(\rho_{\boldsymbol{\nu\mu}}^2 + z_{\boldsymbol{nm}}^2)^{5/2}} = \frac{1}{h}(\mathcal{B}_1 + \mathcal{B}_2 + \mathcal{B}_3),$$

$$\mathcal{B}_1 = -\frac{3}{2\pi}\int dx'dy' \rho^2 e^{-2\imath\alpha} \int_0^h dz \frac{h-z+a_0}{(\rho^2+z^2)^{5/2}} = \frac{1}{2\pi}\int_0^{2\pi} d\alpha e^{-2\imath\alpha}\left[P - \sqrt{P^2+h^2} + \frac{a_0 h}{\sqrt{P^2+h^2}} - 2(h+a_0)\ln\frac{\sqrt{P^2+h^2}-h}{P}\right],$$

$$\mathcal{B}_2 = -\frac{3a_0^4}{8\pi}\sum_{\substack{\boldsymbol{\mu} \\ r_{\boldsymbol{nm}} \neq 0}} \frac{e^{-2\imath\alpha}}{\rho_{\boldsymbol{\nu\mu}}^3} \approx \frac{3a_0^2}{8\pi}\int_0^{2\pi} \frac{e^{-2\imath\alpha}d\alpha}{P}, \quad \mathcal{B}_3 = -\frac{3a_0^2}{8\pi}\int dx'dy' \frac{\rho^2 e^{-2\imath\alpha}}{(\rho^2+h^2)^{5/2}} = \frac{a_0^2}{8\pi}\int_0^{2\pi} d\alpha e^{-2\imath\alpha}\frac{3P^2+2h^2}{(P^2+h^2)^{3/2}}. \quad \text{(B7)}$$

Finally, the coefficient of effective anisotropy $\mathcal{B}(x,y)$ takes the form (15b). As a result, the dipolar energy (B1) can be expressed as Eq. (14).

Note that for the circular system, one can obtain exact expressions for the coefficients $\mathcal{A}$ and $\mathcal{B}$. Let us first find the coefficient $\mathcal{A}$. Assuming that $h \gg a_0$ (or, equivalently, $a_0 \to 0$), one can rewrite the coefficient $\mathcal{A}$ [see Eq. (B4)] as follows:

$$\mathcal{A}(\xi)=\frac{1}{3}+\frac{1}{4\pi\varepsilon}[I_A(2\varepsilon)-I_A(0)],\quad I_A(x)=\int_0^{2\pi}d\alpha\int_0^1\frac{\xi' d\xi'}{\sqrt{\xi^2+\xi'^2+x^2-2\xi\xi'\cos\alpha}},$$

$$I_A(x)=\frac{2}{\sqrt{x^2+(\xi+1)^2}}\{[x^2+(\xi+1)^2]E(\mu)+[1-x^2-\xi^2]K(\mu)+F_+(x)+F_-(x)\}-2\pi x,$$

$$F_\pm(x)=x^2\frac{\sqrt{x^2+\xi^2}\mp 1}{\sqrt{x^2+\xi^2}\pm\xi}\Pi(\nu_\pm|\mu),\quad \mu=\frac{4\xi}{x^2+(1+\xi)^2},\quad \nu_\pm=\frac{2\xi}{\xi\pm\sqrt{x^2+\xi^2}},\tag{B8}$$

where $\Pi(\nu_\pm|\mu)$ is the complete elliptic integral of the third kind.[25]

To calculate the in-plane anisotropy coefficient $\mathcal{B}$ [see Eq. (B7)], it is convenient to use the following relations:

$$\mathrm{Re}[\mathcal{B}e^{-2\imath\chi}]=-\frac{a_0^4}{2\pi h}\bar{B}_{\boldsymbol{\nu}}=-\frac{1}{2\pi h}\int_0^h dz(h-z)I_z(x),$$

$$I_z(x)=3\int dx'dy'\frac{(x-x')^2-(y-y')^2}{(\rho^2+z^2)^{5/2}}=\int dx'dy'\left(\frac{\partial^2}{\partial y\partial y'}-\frac{\partial^2}{\partial x\partial x'}\right)\frac{1}{\sqrt{\rho^2+z^2}}\equiv\int_\Omega[\boldsymbol{\nabla}'\times\boldsymbol{F}]\cdot d\boldsymbol{\sigma}=\oint_{\partial\Omega}\boldsymbol{F}\cdot d\boldsymbol{l}',$$

$$\boldsymbol{F}=\boldsymbol{e}_z\times\boldsymbol{\nabla}\frac{1}{\sqrt{(x-x')^2+(y-y')^2+z^2}}.\tag{B9}$$

For a circular system $d\boldsymbol{l}'=Rd\chi'(-\boldsymbol{e}_x\sin\chi'+\boldsymbol{e}_y\cos\chi')$, hence

$$I_z(x)=R\int_0^{2\pi}d\chi'\left[\frac{\partial}{\partial y}\sin\chi'-\frac{\partial}{\partial x}\cos\chi'\right]\frac{1}{\sqrt{r^2+R^2-2rR\cos(\chi-\chi')+z^2}}=rR\cos(2\chi)\frac{\partial}{\partial r}\left[\frac{1}{r}\int_0^{2\pi}\frac{\cos\alpha d\alpha}{\sqrt{r^2+R^2-2rR\cos\alpha+z^2}}\right].$$

Taking into account that $\mathrm{Im}\,\mathcal{B}=0$ for the circular system, one can calculate finally the effective in-plane anisotropy coefficient $\mathcal{B}$ as follows:

$$\mathcal{B}(\xi)=\frac{1}{2\pi\varepsilon}[I_B(2\varepsilon)-I_B(0)],\quad I_B(x)=c_1K(\mu)+c_2E(\mu)+c_3\Pi\left(\frac{4\xi}{(1+\xi)^2}\middle|\mu\right),$$

$$c_1=\frac{2-2x^2-\xi^2-(x^2+\xi^2)^2}{3\xi^2\sqrt{x^2+(1+\xi)^2}},\quad c_2=\frac{(x^2+\xi^2-2)\sqrt{x^2+(1+\xi)^2}}{3\xi^2},\quad c_3=\frac{x^2(1-\xi)}{\xi^2(1+\xi)\sqrt{x^2+(\xi+1)^2}}.\tag{B10}$$

The dipolar energy W_d [see Eq. (26)] for the disk-shaped system can be presented in the form $W_d=W_d^0+\tilde{W}_d$, where

$$\tilde{W}_d=\frac{1}{R^2}\int d^2x[\tilde{\mathcal{A}}(r)+\mathcal{B}(r)\cos 2(\phi-\chi)]\sin^2\theta\tag{B11}$$

and $W_d^0=-2R^{-2}\int d^2x\mathcal{A}(r)$ being the isotropic part; the effective easy-plane anisotropy parameter $\tilde{\mathcal{A}}=3\mathcal{A}$.

APPENDIX C: CONFIGURATIONAL ANISOTROPY FOR A HALF-PLANE AND A SQUARE PRISM

We start here with the problem for a half-plane. Consider the large scale behavior of the dipolar energy given by the in-plane effective anisotropy $\mathcal{B}(x,y)$ [see Eq. (19)]. Straightforward calculations lead to the effective anisotropy constant for the upper half-plane

$$\mathcal{B}(x,y)\equiv\mathcal{B}(y_0)=\frac{1}{2\pi}\int_{-\infty}^{\infty}dxy_0(y_0^2-x^2)\frac{\mathcal{F}(P,h)}{P^4}$$

$$=\frac{y_0}{2\pi h}\ln\frac{y_0^2}{y_0^2+h^2}+\frac{1}{\pi}\arctan\frac{h}{y_0},\tag{C1}$$

where we choose the origin of the local reference frame at the boundary of the domain, at $(x,y)=(0,0)$, y_0 denotes the distance from the boundary, and $P=\sqrt{x^2+y_0^2}$. One can see that $\mathcal{B}$ does not depend on x, it takes only positive real values; hence, $\arg\mathcal{B}=0$ for *any* distances y_0 from the boundary. This means that the in-plane spin angle ϕ is always parallel to the half-plane edge. Using Eqs. (19b), (19c), and (C1), we found that the main contribution to Eq. (C1) is provided by the boundary domain $x\in[-R_0;R_0]$ with $R_0\sim\sqrt{y_0h}$. Since this domain collapses to a point when $y_0\to 0$, we conclude that for any geometry, the in-plane spin distribution is paral-

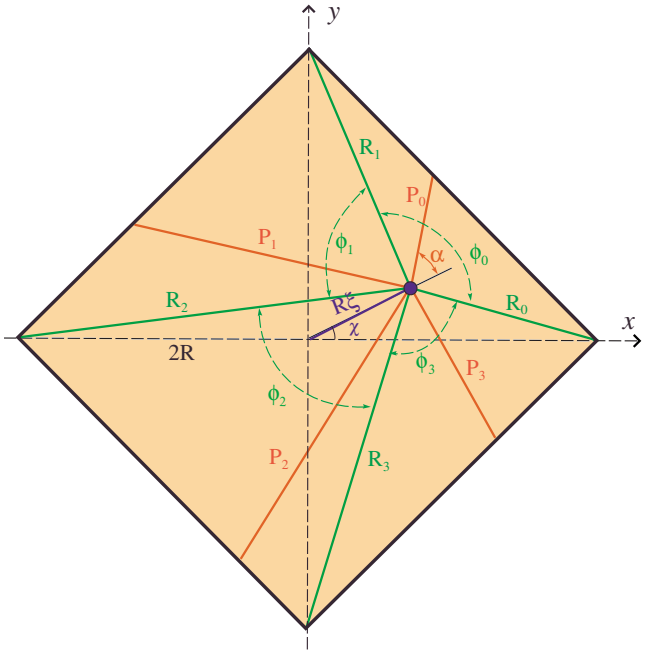

FIG. 6. (Color online) Arrangement of coordinates in the local reference frame for the prism-shaped particle.

lel to the boundary near the edge. If the curvature radius of the sample boundary is larger than R_0, then spins are parallel to the boundary over a distance smaller than R_0^2/h. One should remember that this conclusion is adequate for regions where exchange interaction has no principal influence.

Let us consider now the configurational anisotropy for the square prism, which has the diagonal $2R$ (see Fig. 6). It is convenient to use the local reference frame in the same way as in Sec. II A. The relative polar coordinates are defined as follows:

$$R_n = R\sqrt{1+\xi^2-2\xi\cos(n\pi/2-\chi)},$$

$$\varphi_n = \arccos\frac{R_n^2+R_{n+1}^2-2R^2}{2R_nR_{n+1}},$$

$$P_n = \frac{R_nR_{n+1}}{R\sqrt{2}}\frac{\sin\varphi_n}{\cos[\alpha+\chi-(2n+1)\pi/4]}, \tag{C2}$$

where $\xi=\sqrt{x^2+y^2}/R$. Now we are able to compute the magnetization distribution on a large scale, which follows from the minimization condition (20). Straightforward calculations give

$$\phi = \chi+\frac{\pi}{2}-\frac{1}{2}\arg\mathcal{B}, \tag{C3}$$

$$\mathcal{B} = \frac{1}{2\pi}\left[\int_{\psi_0-\varphi_0}^{\psi_0} e^{-2\imath\alpha}\mathcal{F}(P_0,h)d\alpha + \sum_{j=1}^{3}\int_{\psi_{j-1}}^{\psi_j} e^{-2\imath\alpha}\mathcal{F}(P_j,h)d\alpha\right], \tag{C4}$$

$$\psi_j = \psi_0+\sum_{i=1}^{j}\varphi_i, \tag{C5}$$

$$\psi_0 = \frac{3\pi}{4}-\chi-\arcsin\left(\frac{R_0\sin\varphi_0}{R\sqrt{2}}\right), \tag{C6}$$

where $\mathcal{F}(P_i,h)$ is defined by Eq. (19c).

*Corresponding author. denis_sheka@univ.kiev.ua

[1] A. Hubert and R. Schäfer, *Magnetic Domains* (Springer-Verlag, Berlin, 1998).
[2] R. Skomski, J. Phys.: Condens. Matter **15**, R841 (2003).
[3] S. D. Bader, Rev. Mod. Phys. **78**, 1 (2006).
[4] R. P. Cowburn, J. Magn. Magn. Mater. **242-245**, 505 (2002).
[5] W. F. Brown, Jr., *Micromagnetism* (Wiley, New York, 1963).
[6] A. Aharoni, *Introduction to the Theory of Ferromagnetism* (Oxford University Press, New York, 1996).
[7] E. Stoner and E. Wohlfarth, Philos. Trans. R. Soc. London, Ser. A **240**, 599 (1948).
[8] N. A. Usov and S. E. Peschany, J. Magn. Magn. Mater. **110**, L1 (1992).
[9] R. P. Cowburn, A. O. Adeyeye, and M. E. Welland, Phys. Rev. Lett. **81**, 5414 (1998).
[10] B. A. Ivanov and E. V. Tartakovskaya, JETP Lett. **98**, 1015 (2004).
[11] N. A. Usov and S. E. Peschany, Fiz. Met. Metalloved. **78**, 13 (1994).
[12] V. E. Kireev and B. A. Ivanov, Phys. Rev. B **68**, 104428 (2003).
[13] O. Tchernyshyov and G.-W. Chern, Phys. Rev. Lett. **95**, 197204 (2005).
[14] R. P. Cowburn and M. E. Welland, Phys. Rev. B **58**, 9217 (1998).
[15] G. Gioia and R. D. James, Proc. R. Soc. London, Ser. A **453**, 213 (1997).
[16] A. Desimone, Meccanica **30**, 591 (1995).
[17] A. Desimone, R. V. Kohn, S. Müller, and F. Otto, Commun. Pure Appl. Math. **55**, 1408 (2002).
[18] R. Kohn and V. Slastikov, Proc. R. Soc. London, Ser. A **461**, 143 (2005).
[19] R. V. Kohn and V. V. Slastikov, Archive Ration. Mech. Anal. **178**, 227 (2005).
[20] R. Moser, Archive Ration. Mech. Anal. **174**, 267 (2004).
[21] M. Kurzke, Calculus Var. Partial Differ. Equ. **26**, 1 (2006).
[22] B. A. Ivanov and C. E. Zaspel, Phys. Rev. Lett. **94**, 027205 (2005).
[23] A. I. Akhiezer, V. G. Bar'yakhtar, and S. V. Peletminskiĭ, *Spin Waves* (North-Holland, Amsterdam, 1968).
[24] J. C. S. Lévy, Phys. Rev. B **63**, 104409 (2001).
[25] M. Abramowitz and I. A. Stegun, *Handbook of Mathematical Functions with Formulas, Graphs, and Mathematical Tables* (Dover, New York, 1964).
[26] R. I. Joseph, J. Appl. Phys. **37**, 4639 (1966).
[27] A. Aharoni, J. Appl. Phys. **68**, 2892 (1990).

[28] G. M. Wysin, Phys. Rev. B **49**, 8780 (1994).
[29] B. A. Ivanov and D. D. Sheka, Low Temp. Phys. **21**, 881 (1995).
[30] V. P. Kravchuk, D. D. Sheka, and Y. B. Gaididei, J. Magn. Magn. Mater. **310**, 116 (2007).
[31] R. Höllinger, A. Killinger, and U. Krey, J. Magn. Magn. Mater. **261**, 178 (2003).
[32] *The Object Oriented Micromagnetic Framework*, developed by M. J. Donahue and D. Porter, NIST. We used the 3D version of the 1.2α2 release (http://math.nist.gov/oommf/).